Probabilistic Graphical Model of SPECT/MRI

Stefano Pedemonte[1], Alexandre Bousse[2], Brian F. Hutton[2], Simon Arridge[1], and Sebastien Ourselin[1]

[1] The Centre for Medial Image Computing, UCL, London, United Kingdom
[2] Institute of Nuclear Medicine, UCL Hospitals NHS Trust, London, United Kingdom

Abstract. The combination of PET and SPECT with MRI is an area of active research at present time and will enable new biological and pathological analysis tools for clinical applications and pre-clinical research. Image processing and reconstruction in multi-modal PET/MRI and SPECT/MRI poses new algorithmic and computational challenges. We investigate the use of Probabilistic Graphical Models (PGM) to construct a system model and to factorize the complex joint distribution that arises from the combination of the two imaging systems. A joint generative system model based on finite mixtures is proposed and the structural properties of the associated PGM are addressed in order to obtain an iterative algorithm for estimation of activity and multi-modal segmentation. In a SPECT/MRI digital phantom study, the proposed algorithm outperforms a well established method for multi-modal activity estimation in terms of bias/variance characteristics and identification of lesions.

Keywords: Molecular Imaging, Emission Tomography, Multi-modality, Bayesian Networks

1 Introduction

Algorithms for stochastic image reconstruction in Emission Tomography (PET and SPECT) are widespread in research and clinical applications for the accuracy they can provide by taking into account photon count statistics and detailed system models. Common formulations of such algorithms rely on iterative procedures in order to find an approximation of the spatial distribution of radiopharmaceutical activity that is most likely to have generated the detected photon interaction events. Low photon count and approximated system models heavily limit the resolution in emission tomographic imaging; many publications have focused on multi-modality enhanced reconstruction, where information from an intra-patient anatomical image (CT, MRI) improves the estimate of activity. Such methods are based on the assumption that activity is related to the underlying anatomy, which is linked to the CT and MRI image intensity. Methods in the literature fall within three main categories: methods that favor a piecewise uniform reconstruction by segmenting the anatomical image and subsequently applying a smoothing prior within each identified region; methods that explicitly extract boundary information from the anatomical image and relax the effect of

a global smoothing prior across the identified edges; methods based on information theoretic similarity functionals [1].
The last category has proven particularly interesting, as the involved functionals do not require either explicit segmentation nor boundary extraction from the anatomical image, steps that are inherently sensitive to noise because of selection of high frequency components of the image. The introduction of anatomical prior information via these functionals has been shown to improve the *a posteriori* estimate of activity, by reducing its *bias* and sensitivity to noise [1]. However such methods are uninformed about the imaging processes and present intrinsic problems due to the existence of multiple solutions, which determine estimates of the activity inconsistent with boundary information in the anatomical image.

In this work we develop a joint generative model that captures the complex interactions of high dimensional variables in a combined system for Emission Tomography and MRI. The interdependence of the two imaging modalities is explained by the existence of a hidden state.

Similar generative models based on a hidden state have been adopted recently in multi-modal imaging by Venkataraman *et al.* for joint estimation of brain connectivity from functional MRI (fMRI) and diffusion weighted imaging (DWI) [4] and by Hiltunen *et al.* in single-modality diffuse optical tomography for combined reconstruction-classification [5]. Earlier work on maximum a posteriori joint estimation of function and anatomy was developed by Sastry and Carson [6] who introduced a tissue composition model based on a finite mixture and Rangarajan *et al.* [7] who introduced an iterative scheme for the same model, based on maximization of mutual information.

2 Methods

Modeling the system with a PGM allows us to obtain an iterative algorithm for estimation of activity from the factorization of the joint probability distribution associated to the graphical model [3]. In the following a PGM for the multimodal system is obtained by combining two models of the separate modalities by the use of a latent anatomical/functional state.

2.1 Probabilistic Graphical Model of SPECT

Let the radio-pharmaceutical activity within the region of interest of the patient's body be a continuous function denoted by $\tilde{y}$. In order to readily discretise the reconstruction algorithm, it is convenient to imagine that the activity is in the first place discrete in space. Let us approximate $\tilde{y}$ by a set of point sources $y = y_b, b \in \{1, \ldots, N_b\}$ displaced on a regular grid.
Given that each point source emits radiation at an average rate y_b proportional to the local density of radio-tracer and emission events in a same voxel are not time correlated, the number of emissions in the unit time from within voxel b is a Poisson distribution of expected value y_b. The geometry of the system and attenuation in the patient determine the probability p_{bd} that a photon emitted

in b is detected at detector pixel d (assuming binned detection). From the sum property of the Poisson distribution, the photon count in d is Poisson distributed with expected value $\sum_b p_{bd} y_b$. Given activity y, the probability to observe counts z_d in d is:

$$p(z_d|y) = \mathcal{P}(\sum_b p_{bd} y_b, z_d) \tag{1}$$

As activity determines counts, counts in each of the detector bins d are independent conditionally to activity, as expressed by the directed acyclical graph (DAG) in figure 1-A (and by the Global Markov properties if its moralized graph on the right). Given activity y, the probability to observe z is then:

$$p(z|y) = \prod_{d=1}^{N_d} \mathcal{P}(\sum_b p_{bd} y_b, z_d) \tag{2}$$

2.2 Probabilistic Graphical Model of MRI

Quantitative analysis of tissue properties with MRI is hindered by spatially correlated nonlinearity and varying noise properties of the imaging system. A parametric model that captures the variability of the imaging system, often associated with prior probability distributions of the variables of interest (and eventually of the parameters) is common practice for automated classification of MR images [9]. In this context, models of the imaging system based on finite mixtures assume that the MR image intensity is the uncertain expression, described by a parametric function, of a hidden variable that takes values in a discrete set. Since Rician noise introduced by the MRI imaging system is well approximated, for high SNR, by a Gaussian distribution [9], a Gaussian Finite Mixture model is commonly adopted to represent the MR imaging system. Spatially correlated nonlinearity of the image due to non-uniformity of the magnetic field is not taken into account in the following, though the mixture model may be extended to account for nonlinearity as in [9]. The hidden state in voxel $b \in \{1, 2, \ldots, N_b\}$ is denoted by $k_b = k$, with $k \in \{1, 2, \ldots, N_k\}$. MRI intensity in voxel b is denoted by $x_b = x$, with $x \in \mathbb{R}^+$.

$$p(x_b|k_b) = \mathcal{N}(x_b, \mu_{x_k}, \sigma_{x_k}) \tag{3}$$

Assuming that the prior probability of k is a multinomial distribution $p(k) = \pi_k$ and regarding the unknown parameters as random variables, the mixture model that describes MRI image formation is represented by the Directed Acyclical Graph in figure 1-B. For image segmentation the parameters of this model are commonly estimated by the EM algorithm [9].

2.3 Probabilistic Graphical Model of SPECT/MRI

Since activity is not directly observable, it is not possible to define empirically a model that expresses the interdependence of the two imaging modalities. We postulate that there is an underlying variable that, if known, renders the two

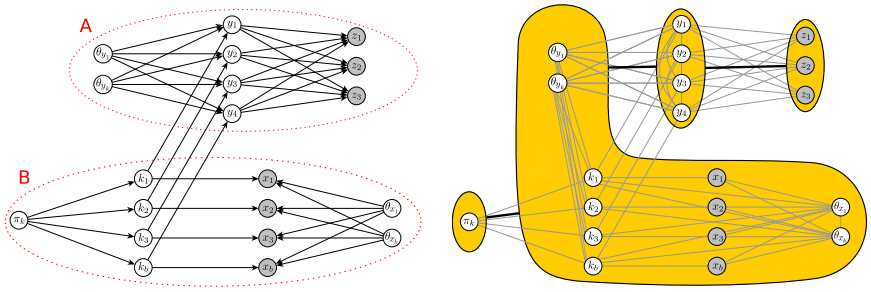

Fig. 1. Directed acyclical graph (left) and moralized Markov Network (right) of the joint generative model for the SPECT/MRI imaging system. Observed quantities are shaded. A hidden anatomical/functional state k_b at each voxel determines activity y and MRI image intensity x; the probability distributions of x and y are independent if the hidden state $k_b = k$ is known and their probability distribution is a parametric function of parameters θ.

images independent. Indexing with $k = \{1, 2, \ldots, N_k\}$ the value of a discrete hidden state, it is assumed that the hidden state in one voxel determines relaxation time and pharmaceutical concentration in the same voxel, which implies that the two variables are independent conditionally to the hidden state $k_b = k$ in b. Accounting for complexity of the reasons of variability of relaxation time and activity in a region defined by a given state, their probability distribution is assumed to be a Gaussian of unknown parameters. The conditional independence $x \leftarrow k \rightarrow y$ implies that $p(x, y)$ is a bivariate Gaussian mixture (GM) with diagonal covariance matrix, represented by the DAG in figure 1-left, which moralizes to the Markov Network on the right. In MRI imaging the intrinsic contrast is produced by differences in proton density and MR relaxation times. However, by selection of appropriate magnetization schemes, signal intensity can be modulated by other important processes such as tissue perfusion, Brownian water motion, tissue oxygenation, mass of molecular groups [8]. The distribution of image intensity is related to the hidden variables that characterized the underlying processes and regions of the image that are distinguishable from others correspond to discrete states of the underlying variable. In the proposed joint model the hidden state captures the relation between activity and MRI intensity and it assumes different meanings depending on the MRI sequence that is adopted. Examples of hidden states are normal tissue with water content corresponding to gray matter, normal tissue with water content of white matter, hypoactive gray matter tissue.

2.4 Inference

The parameters of the model that maximize the joint *pdf* correspond to the state of the system such that the observed quantities (MRI image and photon counts) are more likely to be be observed. Factorization of the joint probability distribution according to the moralized graph in figure 1-right allows us to develop

an iterative method to maximize the joint pdf. Besag introduced the Iterated Conditional Modes (ICM) iterative algorithm to optimize the joint probability of a Markov Network and showed that it provides estimates with always increasing joint probability, thus converging to a local maximum. ICM consists in finding a new estimate of the unknown variable at a node of a Markov Network by maximizing its probability conditional to the neighboring nodes, given their provisional estimates. When applied to each node in turn, moving along the neighboring structure, this procedure defines a single cycle of an iterative algorithm for estimation of all the variables. Considering the factorization in figure 1-right (yellow), ICM consists in finding alternately the parameters of the GM which have highest probability given the activity (i), and the activity with highest probability given the parameters and the SPECT projection data (ii).
(i) Given activity, the DAG in figure 1, represents a bivariate GM with diagonal covariance matrix (because of the condition $y \perp x|k$). We adopt EM to compute a new estimate of the parameters that increases the jpdf as it has a well known formulation for mixture problems [9]: Denoting by π_k the prior probability of k, by μ_{x_k}, μ_{y_k} the expected values and $\sigma_{x_k}, \sigma_{y_k}$ the variances of each class k:

$$\hat{p}_{bk}^{(n+1)} = p(k_b|x_b, y_b) = \frac{\mathcal{N}(x_b, \hat{\mu}_{x_k}^{(n)}, \hat{\sigma}_{x_k}^{(n)})\mathcal{N}(y_b, \hat{\mu}_{y_k}^{(n)}, \hat{\sigma}_{y_k}^{(n)})\hat{\pi}_k^{(n)}}{\sum_{k=1}^{N_k} \mathcal{N}(x_b, \hat{\mu}_{x_k}^{(n)}, \hat{\sigma}_{x_k}^{(n)})\mathcal{N}(y_b, \hat{\mu}_{y_k}^{(n)}, \hat{\sigma}_{y_k}^{(n)})\hat{\pi}_k^{(n)}} \tag{4}$$

$$\hat{\mu}_{x_k}^{(n+1)} = \frac{1}{N_b} \frac{\sum_{b=1}^{N_b} \hat{p}_{bk}^{(n+1)} x_b}{\hat{\pi}_k^{(n+1)}} \qquad \hat{\sigma}_{x_k}^{2^{(n+1)}} = \frac{1}{N_b} \frac{\sum_{b=1}^{N_b} \hat{p}_{bk}^{(n+1)} (\hat{\mu}_{x_k}^{(n+1)} - x_b)^2}{\hat{\pi}_k^{(n+1)}} \tag{5}$$

$$\hat{\mu}_{y_k}^{(n+1)} = \frac{1}{N_b} \frac{\sum_{b=1}^{N_b} \hat{p}_{bk}^{(n+1)} y_b}{\hat{\pi}_k^{(n+1)}} \qquad \hat{\sigma}_{y_k}^{2^{(n+1)}} = \frac{1}{N_b} \frac{\sum_{b=1}^{N_b} \hat{p}_{bk}^{(n+1)} (\hat{\mu}_{y_k}^{(n+1)} - y_b)^2}{\hat{\pi}_k^{(n+1)}} \tag{6}$$

$$\hat{\pi}_k^{(n+1)} = \frac{1}{N_b} \sum_{b=1}^{N_b} \hat{p}_{bk}^{(n+1)} \tag{7}$$

(ii) Given the parameters of the GM, the probability of activity is the product of two terms (figure 1): $p(y|x, \theta, \pi, z) = p(y|x, \theta, \pi)p(z|y)$ where $p(z|y)$ is the Poisson likelihood of equation (2). This is maximized by the One Step Late (OSL) EM algorithm introduced by Green [11]:

$$\hat{y}_b^{(n+1)} = \hat{y}_b^{(n)} \frac{1}{\sum_{d=1}^{N_d} p_{bd} + \frac{\partial}{\partial y_b} \log p(y|x, \theta, \pi)\Big|_{y_b^{(n)}}} \sum_{d=1}^{N_d} \frac{p_{bd}\ z_d}{\sum_{b'=1}^{N_b} p_{b'd}\ \hat{y}_{b'}^{(n)}} \tag{8}$$

$p(y|x, \theta, \pi)$ is obtained by marginalizing over k:

$$p(y|x, \theta, \pi) = \prod_{b=1}^{N_b} p(y_b|\theta, x) = \prod_{b=1}^{N_b} \sum_{k=1}^{N_k} \pi_k p(y_b|k_b, \theta, x) = \prod_{b=1}^{N_b} \sum_{k=1}^{N_k} \pi_k \mathcal{N}(y_b, \mu_{y_k}, \sigma_{y_k})$$

By the chain rule of differentiation, the gradient in (8) simplifies to:

$$\frac{\partial}{\partial y_b} \log p(y|\theta_y) = \sum_{k=1}^{N_k} \pi_k \frac{\mu_{y_k} - y_b}{\sigma_{y_k}^2} p_{bk} \tag{9}$$

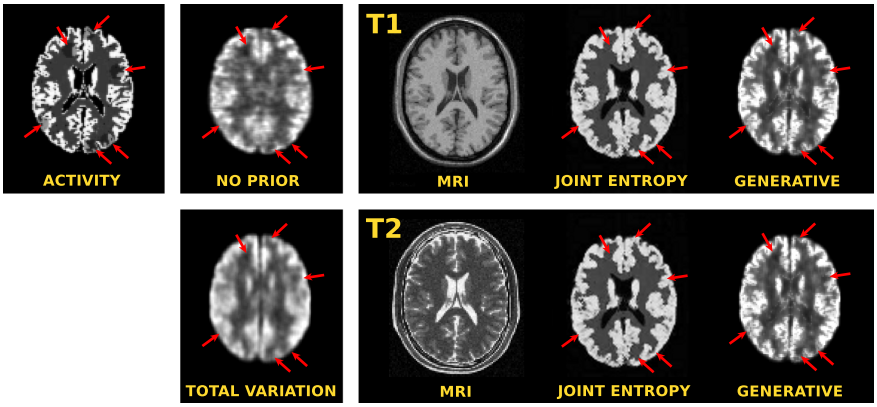

Fig. 2. Central transaxial slice of the activity phantom, the T1 and T2-weighted MRI images and reconstructed activity. The red arrows point to the simulated cold-spots.

3 Validation Study

Synthetic brain data from the BrainWeb [12] database was adopted in order to validate the proposed reconstruction algorithm and compare it with other methods, The MRI and functional imaging processes were decoupled by adopting the normal brain tissue model from the database as ground truth of tissue composition. T1 and T2-weighted MRI images were generated with the BrainWeb simulator, which realistically accounts for noise of the imaging system. The parameters of the simulator were set for noise standard deviation at 3% of the brightest tissue and perfect uniformity of the magnetic field (in accordance with the simplistic GM model). Brain perfusion was simulated by associating typical activity levels to different tissue types, proportionally to partial voxel occupation. Specifically the activity in gray matter was set to a value 4 times higher than in all other tissues. The total number of counts was set to 2.5 Million. 5 spherical cold-spots (red arrows in figure 2) of equal size were simulated at random locations centered on the central transaxial plane by lowering the activity by 30%. The SPECT imaging system was simulated by means of a rotation-based projector with realistic Collimator-Detector Response (CDR) and applying Poisson noise to the projections. The parameters of the imaging system were set to emulate a SPECT imaging system based on GE Infinia with Low Energy High Resolution (LEHR) collimator (size of the detector plane: 540×400 mm; point spread function full width at half maximum (FWHM): $FWHM@20mm = 5.11$ mm, $FWHM@160mm = 9.98$ mm; distance of the detector from the axis of rotation: 133 mm; 120 positions of the gamma camera from 0 to 2π rad). The MRI and activity images were defined on a cubic grid of $(128 \times 128 \times 128)$ voxels.

The number of tissue types was assumed to be $N_k = 4$; μ_{x_k} were initialized to evenly spaced values in the range of intensity of the MRI image; σ_{x_k} were initialized to $1/N_k$ of the image intensity range; μ_{y_k} were initialized to evenly spaced

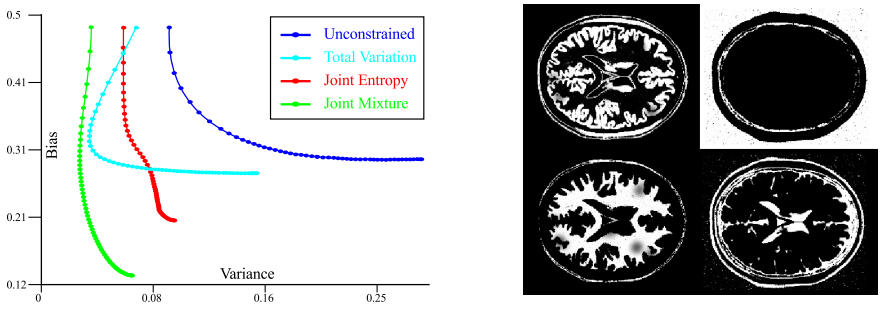

Fig. 3. Left: *bias/variance* at each iteration step for SPECT combined with T1-weighted MRI). Right: Anatomical/functional classification $p(k_b|x_b, y_b)$ for SPECT combined with T1-weighted MRI

values between 0 and the maximum activity assigned to the phantom; σ_{y_k} to $1/N_k$ of the maximum activity assigned to the phantom; the mixing coefficients to $\pi_k = 1/N_k \; \forall \; k \in N_k$. $N1$ and $N2$ were set to 1. A *bias/variance* characterization of the reconstruction algorithms was performed by generating multiple instances of the sinogram data (figure 3-right). The algorithm was launched on 15 realizations of the sinogram. Ensemble *bias* and *variance* were calculated according to the definition in [13].

For comparison, activity was estimated with unconstrained MLEM, with a prior based on total variation (TV) and with a prior based on Joint Entropy (JE) [1]. The hyper-parameters of the TV and JE priors were chosen in order to optimize *bias/variance* as described in [13]. The curves in figure 3-right report *bias/variance* for 100 iterations of each of the methods. The proposed algorithm outperforms all the aforementioned methods in terms of *bias/variance* and identification of lesions by visual assessment. The estimates of the parameters after convergence were inspected and μ_{x_k} and μ_{y_k} demonstrated to converge to large areas of normal activity. None of the classes converged to the cold-spot values. While this issue needs to be addressed by specific solutions, the cold-lesions still appear more visible than with the other reconstruction algorithms. This means that information from the photon counts keeps activity in the cold-spots low, though the anatomical side of the model would tend to suppress them. If the lesions are more visible it is due to overall better redistribution of activity.

4 Discussion

We have introduced a unified framework based on a probabilistic joint generative model of a combined SPECT/MRI imaging system and we have described an iterative algorithm to estimate the parameters of the model, producing an estimate of activity that accounts for prior information from the MRI image along with multi-modal tissue classification. The proposed model is based on the assumption that activity and relaxation time are related because of the existence

of a finite number of states; the phantom has been generated accordingly assigning uniform activity to each of the ground-truth tissue types. The improvement of *bias/variance* and lesion identification over other methods demonstrate that the method works well when the assumption that the model relies on is verified. It is difficult, because of the lack of real life integrated multi-modal imaging systems and of empirical models of the interaction of the pharmaceutical with MRI related tissue properties, to validate the method under realistic conditions. PGM's provide a powerful formalism for model definition and inference in multi-modal imaging systems and offer the potential to integrate estimation at image level with more complex decisioning systems. Extensions of the model proposed in this paper include estimation (correction) of non-linear response of the MRI imaging system, spatial dependence assumption of k and the use of priors for the parameters.

References

1. Atre, A. Vunckx, K., Baete, K., Reilhac, A., Nuyts, J.: Evaluation of different MRI-based anatomical priors for PET brain imaging. In: IEEE Nucl. Sci. Sym. Conf. 1–7, Orlando, October 2009.
2. Leahy, R., Yan, X.: Incorporation of Anatomical MR Data for Improved Functional Imaging with PET. In: Inf. Proc. in Med. Imag. 105–120, Springer, 1991.
3. Scheines, R.: An Introduction to Causal Inference. In: Causality in Crisis?, pp. 185–200, V. McKim and S. Turner (eds.), University of Notre Dame Press.
4. Venkataraman2010, A., Rathi, Y., Kubicki, M., Westin, C.F., Golland, P.: Joint Generative Model for fMRI/DWI and Its Application to Population Studies. In: MICCAI 2010, Part I, 191-199, 2010.
5. Hiltunen, P., Prince, S.J.D., Arridge, S.: A combined reconstruction-classification method for diffuse optical tomography. Phys. in Med. and Biol. 54, 6457–76, 2009.
6. Sastry, S., Carson, R.E.: Multimodality Bayesian algorithm for image reconstruction in positron emission tomography: a tissue composition model. In: IEEE Trans. on Med. Imag. 16(6), 750–61, December 1997.
7. Rangarajan, A., Hsiao, I.T., Gindi, G.: A Bayesian joint mixture framework for the integration of anatomical information in functional image reconstruction. J. of Math. Imag. and Vis. 12(3), 199–217, 2000.
8. Blamire, A.M.: The technology of MRI - the next 10 years? The British J. of Radiology, 81, 601–17, August 2008.
9. Van Leemput, K., Maes, F., Vandermeulen, D., Suetens, P.: Automated model-based tissue classification of MR images of the brain. IEEE Trans. on Med. Imag. 18(10), 897–908, October 1999.
10. Ashburner, J., Friston, K.J.: Unified segmentation. Neuroimage, 26(3), 839–51, July 2005.
11. Green, P.G., Bayesian Reconstructions From Emission Tomography Data Using a Modified EM Algorithm. IEEE Trans. on Med. Imag. 9(1), 84–93, 1990.
12. Brain Web, `http://mouldy.bic.mni.mcgill.ca/brainweb/`
13. Pedemonte, S., Cardoso, M.J., Bousse, A., Panagiotou, C., Kazantsev, D., Arridge, S., Hutton, B.F., Ourselin, S.: Class conditional entropic prior for MRI enhanced SPECT reconstruction. In: IEEE Nucl. Sci. Sym. Conf. 3292–3300, Knoxville, November 2010.